JCEC
THE JOURNAL OF ENGINEERING AND EXACT SCIENCES

OPEN ACCESS

The Journal of Engineering and Exact Sciences – jCEC, Vol. 09 N. 10 (2023)
journal homepage: https://periodicos.ufv.br/jcec
eISSN: 2527-1075
ISSN: 2446-9416

Synthesis and application of modified membranes for efficient cationic and anionic dye elimination

Article Info:
Article history: Received 2023-03-03 / Accepted 2023-12-11 / Available online 2023-12-11
doi: 10.18540/jcecvl9iss10pp17578

Meriem Mansour Hafifi
ORCID: https://orcid.org/0000-0003-0317-9133
Laboratory of SEAMM Faculty of Science and Technology, University of Mostaganem Abdelhamid Ibn Badis (UMAB), B.P. 188, Mostaganem 27000, Algeria
E-mail: meriem_hafifi@yahoo.fr
Abdelkader Chougui
ORCID: https://orcid.org/0000-0001-6450-9277
Ibn Khaldoun University of Tiaret, 14000, Algeria
E-mail: abdelkader.chougui@univ-tiaret.dz
Mohammed Amin Chemrak
ORCID: https://orcid.org/0000-0003-2823-5568
Faculty of Sciences and Technology, University of Tissemsilt, Road of Bougara, Ben Hamouda, Tissemsilt 38004, Algeria
E-mail: ma.chemrak@univ-tissemsilt.dz
Aissa Belouatek
ORCID: https://orcid.org/0000-0002-4480-3919
Laboratory of SEAMM Faculty of Science and Technology, University of Mostaganem Abdelhamid Ibn Badis (UMAB), B.P. 188, Mostaganem 27000, Algeria
E-mail: abelouatek@gmail.com

Abstract
This study focuses on developing ceramic ultrafiltration membranes using locally sourced kaolin clay and feldspar. An active layer composed of graphene and alkoxide is added to enhance the performance of these clay supports. This layer is thin, porous, and can vary in thickness. The support and filter layer's porous properties are characterized using SEM, DRX, ATG/ATD, XPS, and FTIR techniques. Filtration tests are conducted on modified porous tubular supports using cationic and anionic dye solutions. The filtration is performed tangentially at a pressure of 3.5 bar and a processing time of 120 minutes. The retention rates of the colored solutions are measured using a UV-visible spectrophotometer. The results show a 100% retention rate for supranol yellow and orange II at a concentration of 10^{-4} M, while for crystal violet and malachite green, the retention rates are 92.03% and 95.30%, respectively.
Keywords: Ceramic membranes. Filtration. Dye removal. Efficiencies. Sol-gel.

1. Introduction

Environmental pollution is an acute problem on a global scale, caused by the increase in industrial discharges into the environment. Among these discharges, those from the textile dye industry are responsible for nuisances since most are toxic and non-biodegradable. Treatment of these discharges by conventional methods is often ineffective. For this reason, other low-cost methods are used for their elimination, such as membrane filtration, which is the subject of numerous studies (Y. Gan *et al*., 2023; Hafani *et al*., 2021; Men *et al*., 2023; Sutariya *et al*., 2023; Zaiter *et al*., 2020). Membrane processes are viable methods for removing a wide range of pollutants from water (Abbasi & Habibi, 2016). Membrane technology has made great strides in the separation

of dyes and heavy metals thanks to ultrafiltration, nanofiltration and reverse osmosis (Kammakakam & Lai, 2023; Mahmoud & Mostafa, 2023; Pezeshki *et al*., 2023; Ramutshatsha-Makhwedzha & Nomngongo, 2022; Shoshaa *et al*., 2023). Membrane separation processes are a constantly evolving technology due to the wide range of applications and the development of numerous filter materials (G. Gan *et al*., 2023; Li *et al*., 2023; Puertas *et al*., 2023; Rezende Moreira *et al*., 2022). Filtration processes are used in fields such as the chemical industry, food processing, water and effluent treatment, biotechnology and electronics (Chougui *et al*., 2014; Johnson & Singer, 2004). The industrial application of porous ceramic membranes with various advantages such as mechanical, thermal and chemical resistance, controlled microstructure and low pollution of our environment has attracted a lot of attention in the scientific community (Asli, Chougui, *et al*., 2022; Zaiter *et al*., 2015). This study focuses on developing and characterizing a porous ceramic membrane where we have deposited an alkoxide and graphene-based filter layer using the sol-gel technique to remove cationic and anionic dyes.

2. Materials and methods

2.1 Chemicals

The natural elements native to Algeria, such as feldspar and kaolin, were the source of the materials used in this study. Alkoxide (molecular weight: 162.165 g/mol) and graphene (Cn) were purchased from Acros Organics and Sigma-Aldrich, respectively. The feed solutions were prepared using analytical grade chemical components (SY, OII, CV, and MG) acquired from Biochemical Technology Co Ltd. Additionally, only milli-Q grade water was used to make these solutions.

2.2 Preparation of membranes

The tubular support was formulated using a slip of local clay, Kaolin, with particle diameters below 80 micrometers, feldspar, a deflocculant, and water. A deflocculant prevents undesirable agglomerates within the suspension, producing a high-quality membrane pre- and post-sintering (Belouatek *et al*., 2005; Obada *et al*., 2017). The resulting slip was poured into a plaster mould, yielding tubular supports measuring 19cm long with an internal/external diameter of 1.4mm. These supports are intended to provide mechanical support for the filtration layer. Drying was conducted at room temperature for 48 hours to facilitate uniform water evaporation from the mixture and prevent potential cracking. Following drying, a filtration layer was applied to the internal surface of the tubular support using the engobing technique. Subsequently, the support/membrane underwent thermal treatment at 1150°C, ramping up at a heating rate of 5°C/min for 7 hours under an air atmosphere. The selection of 1150°C stemmed from previous studies demonstrating optimal mechanical properties achieved at this temperature (Zhao *et al*., 2013). The sol-gel technique prepared the filter layer from alkoxide (aluminium triethoxide) and graphene (C_n). The filter layer was prepared by the sol-gel method (Zanurin *et al*., 2022)by adding 30 ml of methanol solution, 20 ml of 0.1N HCl solution and 0.2 g of aluminium triethoxide to 5 g of graphene. The sol-graphene suspension was stirred for three hours and maintained at a temperature of 80°C. The acid catalyzed the aluminium triethoxide hydrolysis reaction, and the sol-graphene break was transformed into a gel-graphene. The rest is prepared by adding a solution of acetone and distilled water to graphite powder (chalk lead). The ultrasonic treatment lasts 5 hours; the sheets are separated by mass and surface area, the lighter sheets are found at the top of the suspension (supernatant), and the solution is filtered and dried at 60°C for 24 hours. We obtained two ceramic membranes, CM and GCM, before and after alkoxide and graphene filter layer deposition.

2.3 Characterization of membrane

At room temperature, infrared (IR) spectroscopy investigations were performed in the 400–4000 cm-1 wavenumber range using a Perkin Elmer Spectrum Two FT-IR instrument fitted with ATR (Attenuated Total Reflection) sampling accessories, yielding a 2 cm^{-1} spectral resolution.

A simultaneous TGA-DSC instrument, the STA 449 F5 Jupiter1, was used to perform thermogravimetric analysis (TGA), which was used to assess the membranes' thermal stability. In

an oxygen-rich atmosphere, 10 mg of samples were heated gradually at a rate of 5 °C per minute until they reached 1000 °C for analysis. This analytical method monitors the weight at 5°C per minute in an oxygen-rich atmosphere until it comes to 1000°C. It fluctuates during controlled heating of the specimen. This allows for assessing a material's volatile component content and thermal stability.

The crystallographic phase composition of the microporous membranes was meticulously investigated employing X-ray diffraction (XRD) analysis facilitated by an XPert MPD instrument. A copper (Cu) radiation source, operating at 40 kV, emitting Cu K-alpha radiation with a wavelength (λ) of 1.54 A, was utilized to comprehensively examine the membrane's crystalline structure and phase identification. By applying this specific instrumentation and radiation source, XRD analysis facilitated the detailed characterization and determination of the crystallographic phases within the microporous membranes.

The analysis of scanning electron microscope (SEM) micrographs was conducted employing a ULTRA PLUS scanning electron microscope (JEOL, JMC-6000) operating at an elevated voltage of 15 kilovolts (kV). This instrument was integrated with X-ray photoelectron spectroscopy (XPS), facilitating complementary examination and elemental characterization of the surface morphology and composition of the samples. The SEM analysis, conducted at an increased voltage combined with XPS, allowed for a comprehensive investigation, offering insights into the specimens' topographical features and elemental constituents.

2.4 Ultrafiltration tests

Cross-flow filtration studies were conducted at a TMP of 3.5 bar using tubular membranes (length: 30 cm; inner diameter: 12 mm; outer diameter: 13.4 mm) (a schematic of the filtration unit is depicted in Figure 1).

The dye rejection of three concentrations (10^{-5}, 10^{-4}, 10^{-3} M) of crystal violet (MW= 407,99 g/mol, λ_{max} = 590 g/mol), malachite green (MW= 927,02 g/mol, λ_{max} = 616 nm), supranol yellow (MW= 452 g/mol, λ_{max} = 402 nm), and orange II (MW = 350 g/mol, λ_{max} = 484 nm) solutions was filtered tangentially for two hours at a TMP of 3.5 bar was determined according to (Chougui *et al*., 2019):

$$R\ (\%) = 100\left(1 - \frac{C_p}{C_F}\right) \quad (1)$$

where R is the dye rejection, [%], C_p is the permeate concentrations, [M], and C_F is the feed concentrations, [M].

The rejection findings presented here are the average of three separate experiments.

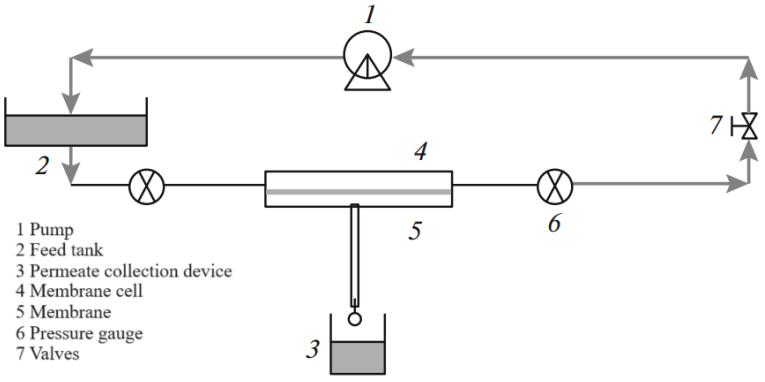

Figure 1 - Cross-flow ultrafiltration unit.

3. Results and discussion

3.1 Membrane characterization

FTIR spectroscopy analysis: Figure 2 shows the FTIR spectra of graphite, graphene and gel-graphene (GCM).

In the GCM spectrum, broadband appears around 3425 cm^{-1}, attributed to the hydroxyl group (Santra *et al*., 2020) present on the surface.

A small peak is observed at 2925 $cm^{-1,}$ which is linked to the (C-H) vibration of CH_3 and CH_2, and another peak at around 1634 cm^{-1} is attributed to the (C = C) bond of graphene. Another band at 1036 cm^{-1} is associated with the stretching of (C-O) (Aouadja *et al*., 2022) and (Al -O-C) or Al-O-Al at around 870 cm^{-1}.

For both graphene and graphite spectra, a single band appeared at 1036 cm^{-1}, attributed to the stretching vibration of C-O cm^{-1}.

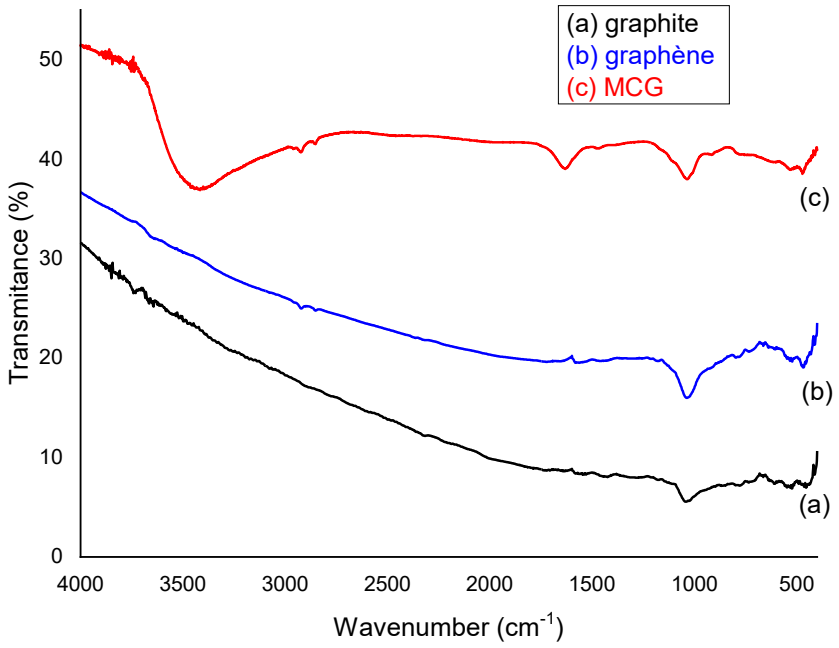

Figure 1 - FTIR spectra of graphite, graphene and gel-graphene (filter layer).

Thermal analysis: Thermal analysis of the filter layer powder (GCM) showed a total weight loss of around 0.6% (Figure 3).

The first weight loss is linked to the departure of physically adsorbed water at around 100°C; a slight weight loss at 200°C is due to the decomposition of oxygen-containing groups; a weight loss at 600°C is attributed to the pyrolysis of the filter layer's alumina groups.

The second weight loss is due to material decomposition between 600°C and 800°C.

An endothermic peak is observed around, accompanied by a loss of mass caused by the elimination of residual water physically adsorbed in the sample.

An exothermic peak is observed at around 700°C due to the decomposition of the material.

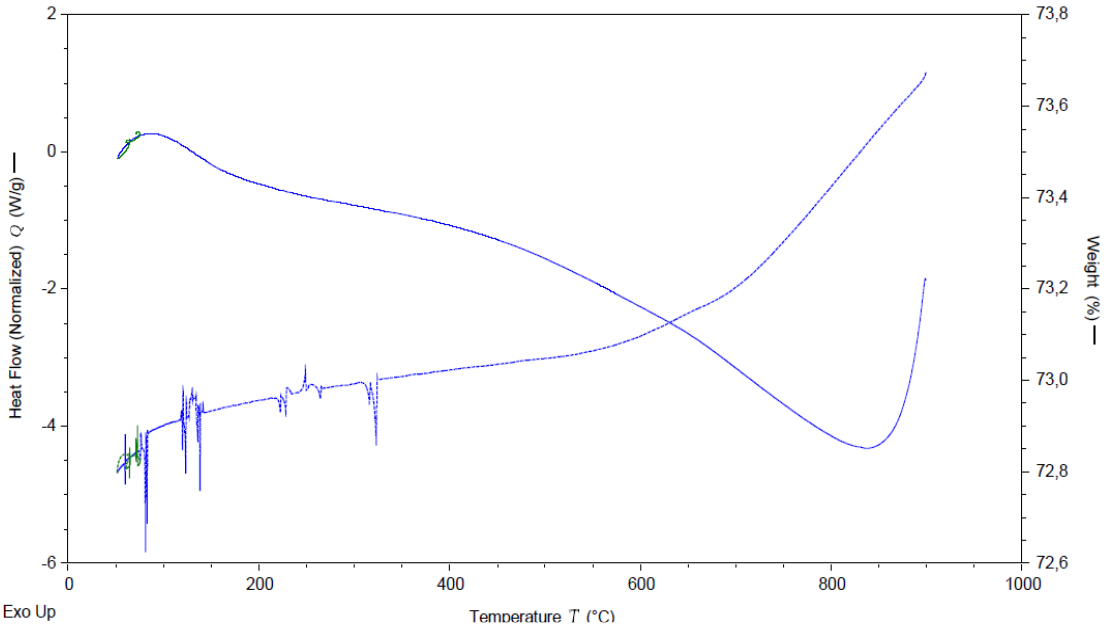

Figure 3 - Thermogravimetric analysis curve of the filter layer.

XRD analysis: XRD spectra of CM and GCM membranes obtained before and after treatment at 1150°C are shown in Figures 4 (a), (b), (c) and (d), respectively.

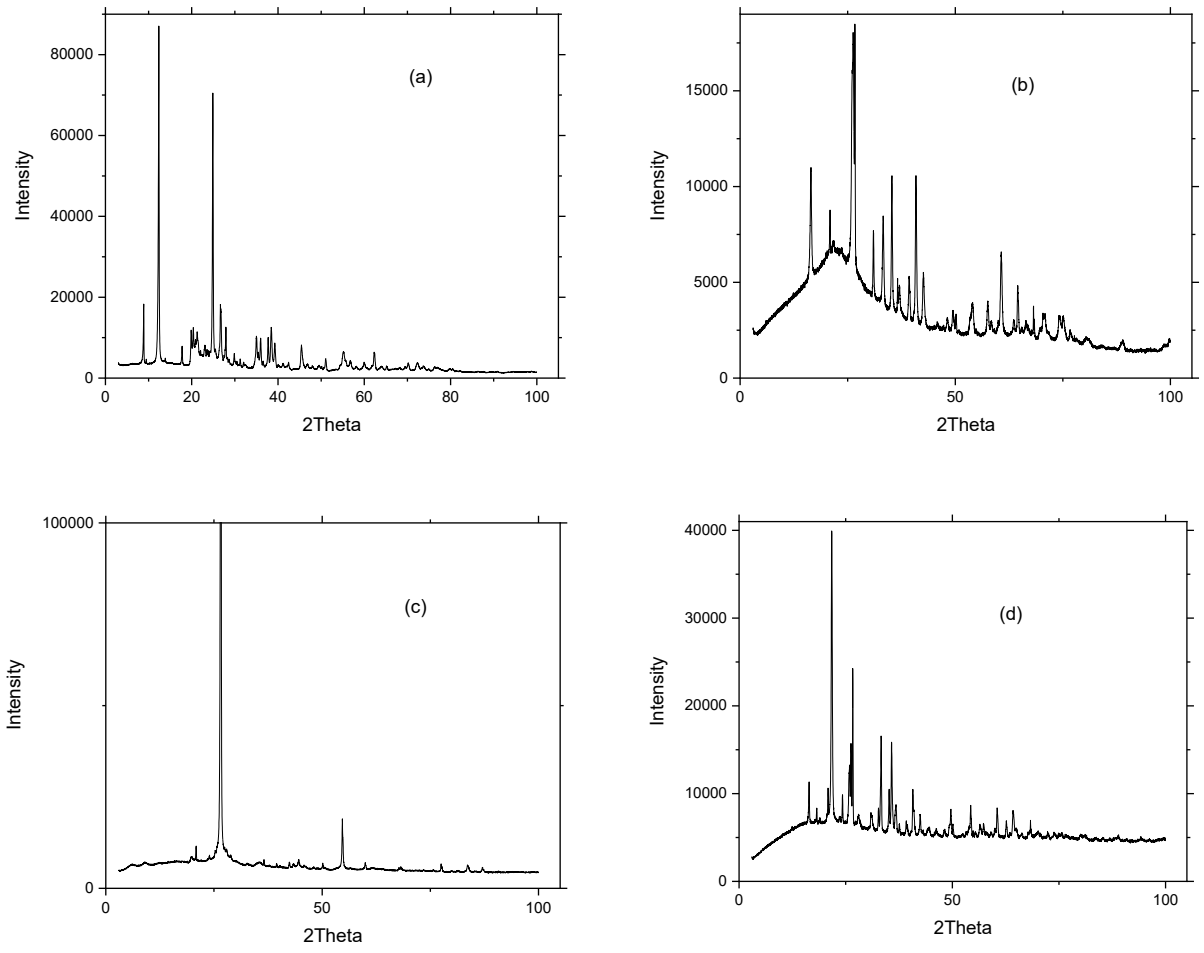

Figure 4 - XRD spectra of (a, b): CM powder before and after 1150°C treatment, (c, d): GCM powder back and after 1150°C treatment.

Determination of the structural phases of raw kaolin by XRD reveals that our clay is made up of a majority phase of kaolinite and quartz, with a fine muscovite fraction. The peaks characteristic of kaolinite (2Θ =12.3° and 24.8°), the peaks that characterize muscovite (2Θ = 8.9 ° and 17.8 °), and quartz (2Θ = 26.5°) are mainly observed. For kaolin treated at 1150°C, the intensity of the peaks becomes increasingly essential, and a literature search has shown that treatment at 1150°C results in the appearance of the characteristic mullite peak (Alsubei *et al*., 2024; Rafya *et al*., 2023), the kaolinite phase has disappeared and the mullite phase [$3Al_2O_3$, $2SiO_2$] is the main mineral present in the powder, meaning that porosity is independent of the phase formed, these identified phases are of great importance due to their promising physical and mechanical properties.

The VRD spectrum of the raw gel-graphene powder (GCM) shows a peak at (2Θ = 28°), which corresponds to the Aluminum peak; we can conclude that the graphene sheets have been covered by the Aluminum particles in the gel-graphene (GCM).

SEM analysis: Figure 5 shows the images of SEM images of the two ceramic membranes before and after coating with the filter layer. The photos show a heterogeneous roughened structure with pores of different sizes and small cavities. On the surface of the support, distinct grains of varying sizes can be observed, corresponding to the presence of mullite and an amorphous mass.

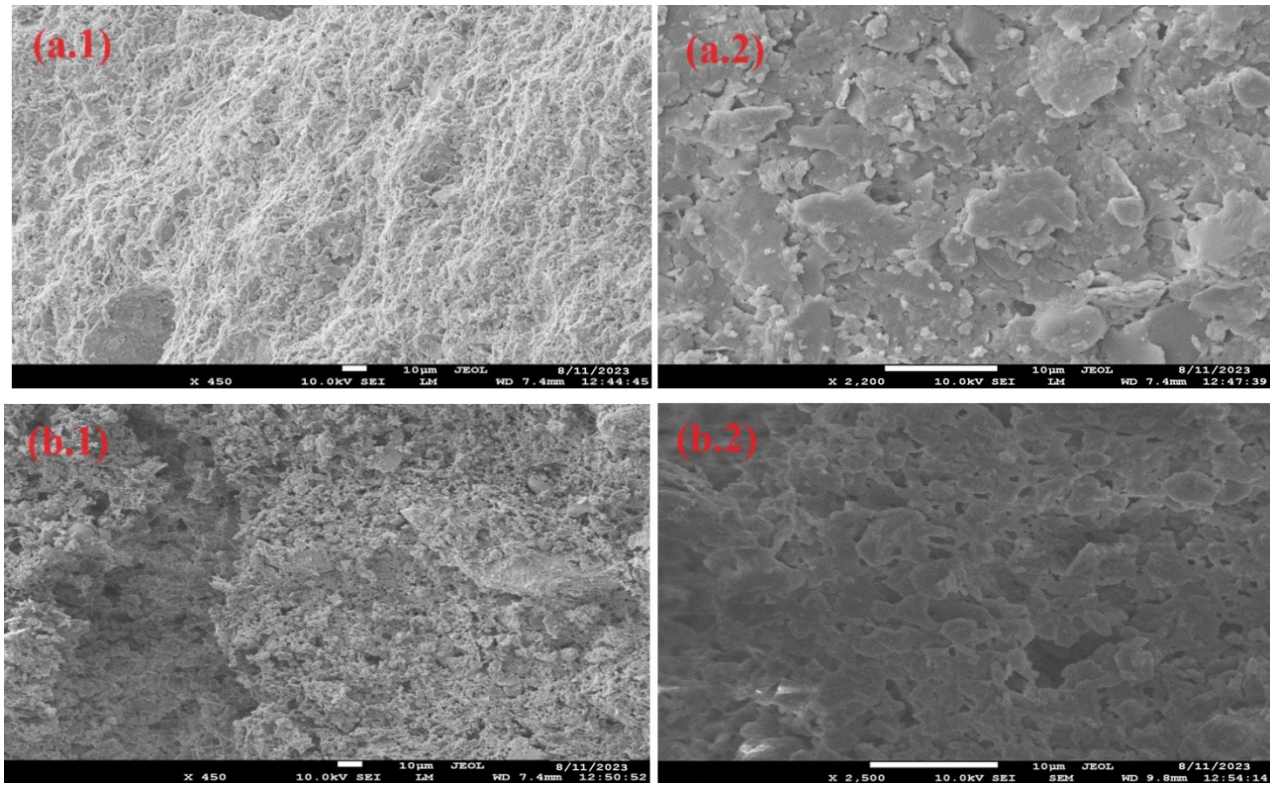

Figure 5 - SEM of the CM membrane (a) and GCM membrane (b).

XPS analysis: Figure 6 shows the XPS spectra of the GCM membrane as can be seen from the survey spectrum; the GCM indicated the scope with peaks Al 2p, C1s, Ca 2p, Na 2p, C1s, Fe 2p and Si 2p. Examination of this spectrum shows two prominent peaks at energies 284.459 and 531.759 eV corresponding to carbon and oxygen, another peak at around 74.159 eV representing aluminium and another for silica at about 102.459 eV. The C 1s mounts can be integrated into two independent sub-bands attributed to the carbon in the (C-C) 284.45 eV and (C-O) 288 eV bonds. In addition, the O 1s peaks at 531.75eV and 532eV could be due to the presence of (C-O) and (AL-O) bond states in the samples. The peak area is proportional to the number of atoms of the element studied (Asli, Mokhtar, *et al*., 2022), and by calculating the respective share of each area, we obtain the atomic composition of the sample. We can see that the percentage of oxygen is 75% and carbon 25%.

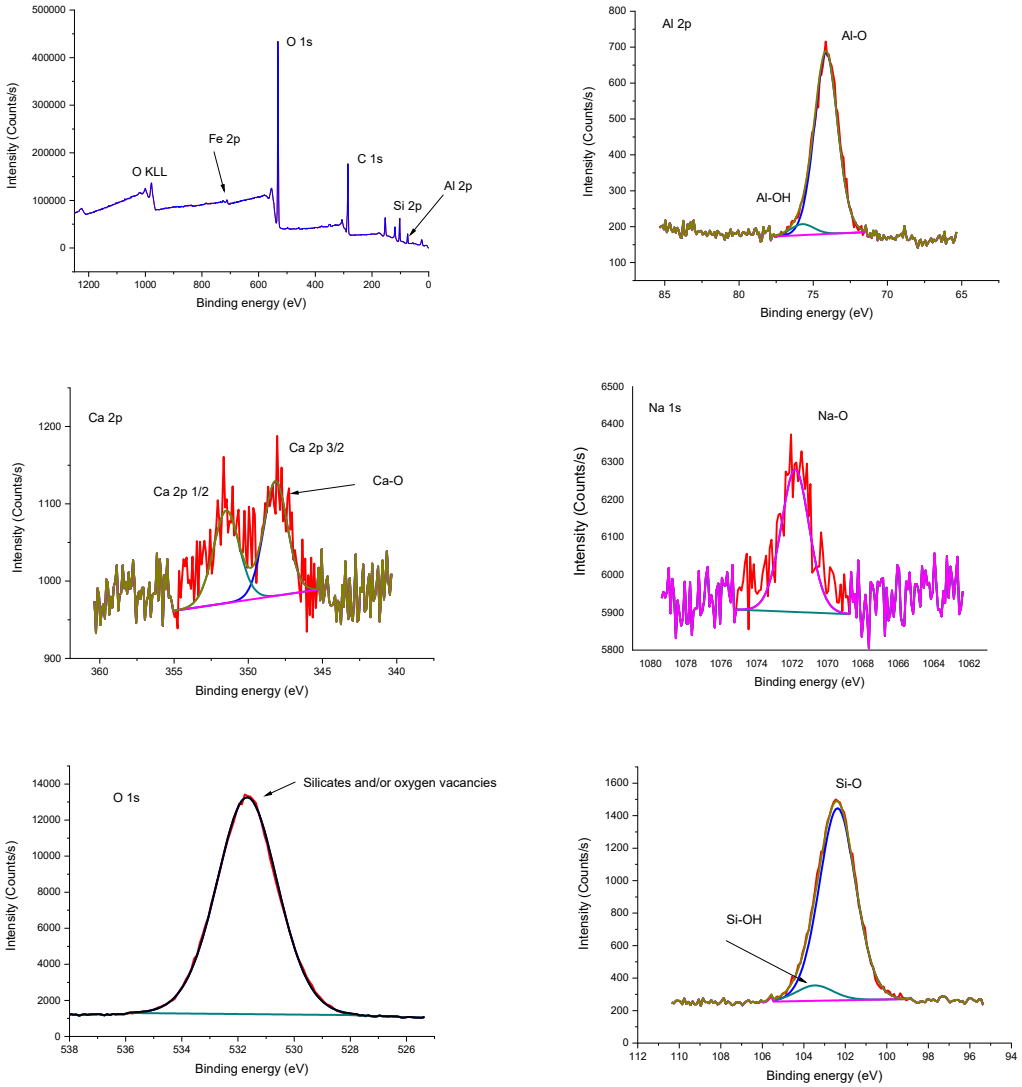

Figure 6 - XPS spectrum of GCM membrane.

3.2 Water flux and permeability

Figure 7 shows the water flows for the CM and GCM membranes. In both cases, water flow varied linearly with TMP, as predicted by Darcy's law (Masturi *et al*., 2018; Oliveira Neto *et al*., 2021). The flux values for the CM membrane vary between 130 L/hm^2 and 490 L/hm^2 for a transmembrane pressure applied between 2 and 4 bar. For the GCM membrane, the flux values of the permeate are 40.019 L/hm2 at 2 bars and 78.431 L/hm^2 at 4 bars. The difference in fluxes obtained is due to the surface morphology of the two membranes. Therefore, the pore radius and the porosity thickness ratio are more significant for the CM membrane than the GCM membrane.

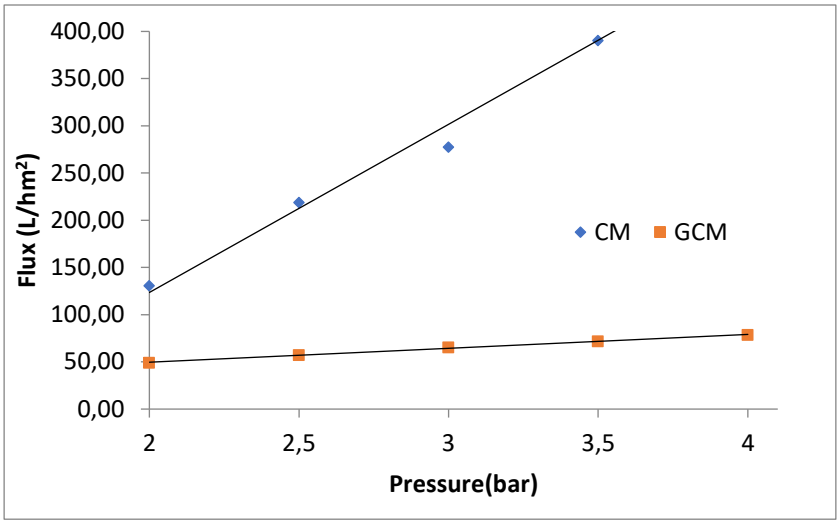

Figure 7- Water flux vs. transmembrane pressure (TMP)

Figure 8 shows the evolution of flow values over time for the same water conditions and operating pressure. A decrease in flow was observed for both membranes during the first 30 minutes of operation before the steady state. The reduction in flow through the CM membrane is more significant than that through the GCM membrane due to the trapping of fine particles on the membrane surface. The clogging effect defines this phenomenon, and the pore size of the GCM membrane is smaller than that of the CM.

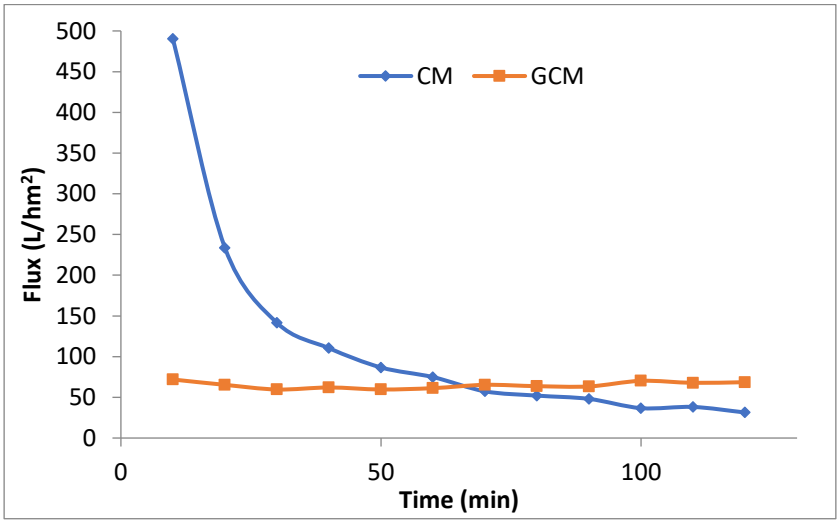

Figure 8- Changes in permeation flux over time for various feed solutions over CM and GCM membranes (TMP = 3.5 bar).

3.2 Dye rejection

Figure 9 illustrates the temporal progression of dye rejection, specifically (a) supranol yellow, (b) orange II, (c) malachite green, and (d) crystal violet. This examination pertains to the diverse concentrations (10^{-5}, 10^{-4}, 10^{-3} M) within the feed solutions administered to CM and GCM membranes.

The activated membrane (GCM) achieves a maximum retention rate of 100% for supranol yellow over 2-hour treatments at concentrations $C_F=10^{-4}$ M and $C_F= 10^{-5}$ M. This heightened removal efficacy stems from charge interactions between the dye ion and the negatively charged membrane. Conversely, the non-activated membrane (MC) exhibits lower retention rates, ranging between 80.67% and 86.9%. This disparity is attributed to the comparatively small size of the dyes relative to the pores within the ceramic membrane.

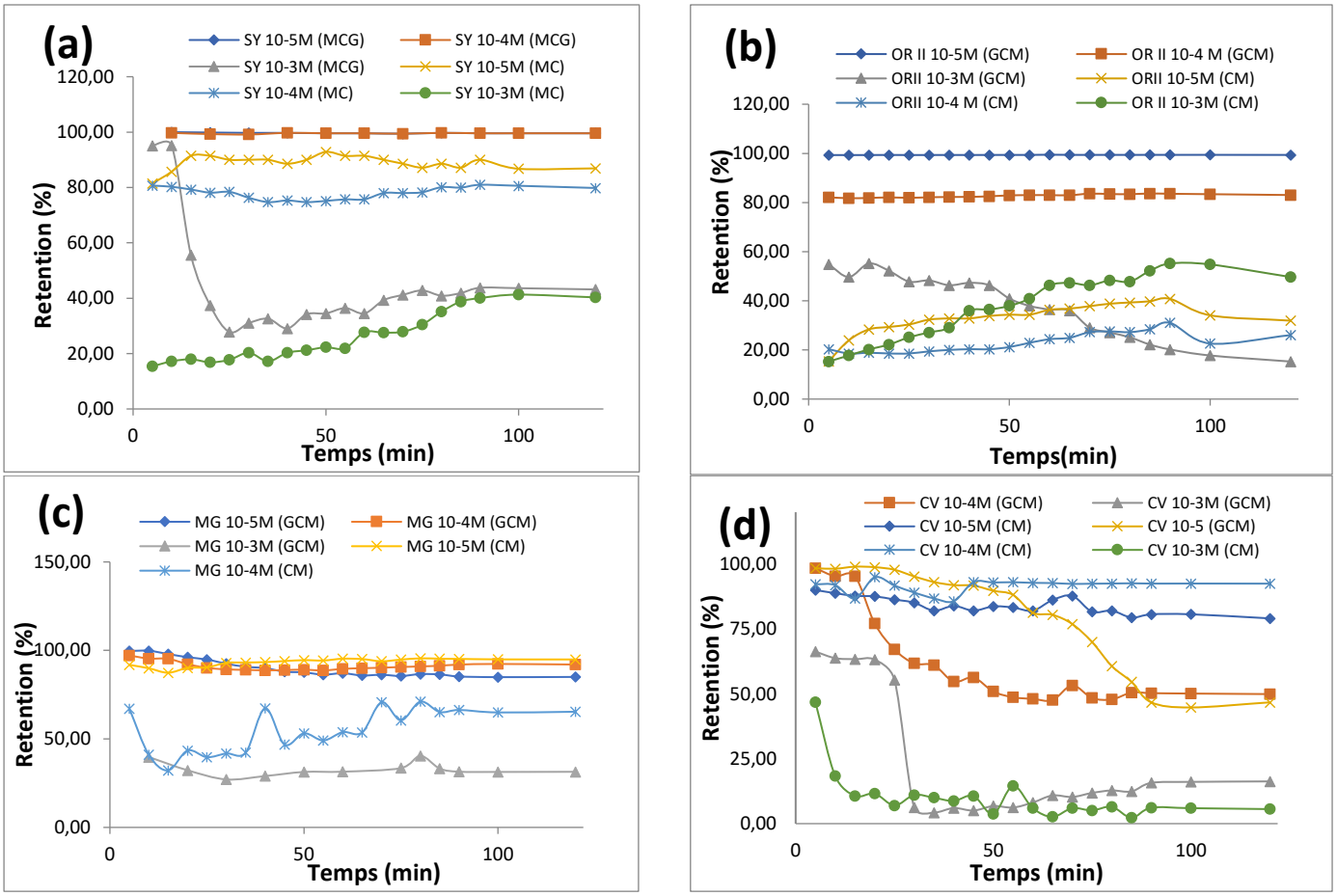

Figure 9 - The temporal evolution of dye rejection ((a) supranol yellow, (b) orange II, (c) malachite green, (d) crystal violet) is examined concerning varying concentrations (10^{-5}, 10^{-4}, 10^{-3} M) of feed solutions applied to CM and GCM membranes.

The retention efficacy of orange II dye through the activated membrane (GCM) achieves complete removal, reaching 100% within a 2-hour treatment duration for a concentration (C_F) of 10^{-5} M while demonstrating an 80% retention rate at $C_F = 10^{-4}$ M. This substantial retention is ascribed to the selective adsorption of the dye, both on the membrane's surface and within its porous structure. Conversely, the orange II retention rate for the non-activated CM membrane varies between 20.29% and 18.55% for the concentrations 10^{-5} M and 10^{-4} M, rising to 31.51% and 26.03%. This variation is due to adsorption by clogging or blocking.

The activated GCM membrane exhibits maximal retention rates of 98.82% and 95.30% for crystal violet at concentrations of 10^{-5} M and 10^{-4} M within the initial 20-minute treatment period. However, this retention subsequently diminishes to stabilize at 46.74% and 50.49%, respectively. Conversely, the non-activated CM membrane initially retains 90.02% at 10^{-5} M, reducing to 54.63% at 10^{-4} M. Over a 120-minute treatment duration, an elimination rate of 92.26% is observed, owing to the selective adsorption of crystal violet dye on the membrane's surface and within its pores.

Applying the activated membrane (GCM) initially results in a retention rate of 99.81% in the initial treatment phase, progressively declining to 85.02% at the 10^{-5} M concentration and 92.03% at the 10^{-4} M concentration. In contrast, the non-activated MC membrane exhibits comparatively lower initial retention of 91.86% after 10 minutes of treatment, stabilizing at a consistent value of 95.52% for a 10-5 M concentration.

4. Conclusion

Implementing ceramic membranes derived from locally obtained kaolin signifies a substantial advancement in dye removal within the industrial domain. Their distinctive adsorption characteristics, complemented by their sustainability and cost-effectiveness, establish them as a crucial asset in alleviating the environmental repercussions of industrial dyeing processes.

The present study encompasses the creation of a ceramic substrate and a microfiltration membrane utilizing indigenous clay, namely kaolin and feldspar, readily available within our geographical scope. The active membrane was applied onto the substrate employing the slip casting technique, complemented by adding an active layer comprising graphene and alkoxide.

The retention properties of the substrate exhibit significance in dye filtration, where retention efficiency correlates significantly with the molecular weight of the species within the filtered dye solutions. The evolution of retention depicts the interactions between dye species and material surface. Notably, the retention rates achieved 100% for Supranol Yellow and Orange II at a concentration of 10^{-4} M, while for Crystal Violet and Malachite Green, the retention rates attained 92.03% and 95.50%, respectively. The membrane demonstrated commendable efficacy in dye removal, indicating its potential utility for treating industrial effluents, particularly in addressing discharges from textile and tanning industries.

Acknowledgements

We thank the General Directorate for Scientific Research and Technological Development for the valuable material and moral support they extended to the Laboratory of Structure, Elaboration, and Application to Materials.

References

Abbasi, M., & Habibi, M. M. (2016). Optimization and characterization of Direct Blue 71 removal using nanocomposite of Chitosan-MWCNTs: Central composite design modeling. *Journal of the Taiwan Institute of Chemical Engineers*, *62*, 112–121. https://doi.org/10.1016/J.JTICE.2016.01.019

Alsubei, M. D., Reid, B., Aljlil, S. A., Coppens, M. O., & Campos, L. C. (2024). Fabrication and characterization of coated ceramic membranes from natural sources for water treatment applications. *Journal of Membrane Science*, *690*, 122226. https://doi.org/10.1016/J.MEMSCI.2023.122226

Aouadja, F., Bouzerara, F., Guvenc, C. M., & Demir, M. M. (2022). Fabrication and properties of novel porous ceramic membrane supports from the (Sig) diatomite and alumina mixtures. *Boletín de La Sociedad Española de Cerámica y Vidrio*, *61*(5), 531–540. https://doi.org/10.1016/J.BSECV.2021.04.002

Asli, B., Chougui, A., Belouatek, A., & Zaiter, K. (2022). Removal of heavy metals and COD containing leachate by ceramic membranes. *Algerian Journal of Environmental Science and Technology*, *8*(2). https://www.aljest.net/index.php/aljest/article/view/560

Asli, B., Mokhtar, A., & Belouatek, A. (2022). Fabrication and characterization of ceramic hollow shaped from the local kaolin intended for the filtration. *Https://Doi.Org/10.1080/14328917.2022.2059940*, *27*(1), 13–19. https://doi.org/10.1080/14328917.2022.2059940

Belouatek, A., Benderdouche, N., Addou, A., Ouagued, A., & Bettahar, N. (2005). Preparation of inorganic supports for liquid waste treatment. *Microporous and Mesoporous Materials*, *85*(1–2), 163–168. https://doi.org/10.1016/J.MICROMESO.2005.06.007

Chougui, A., Belouatek, A., & Rabiller-Baudry, M. (2019). Synthesis and characterization of new ultrafiltration ceramic membranes for water treatment. *Journal of Water Process Engineering*, *30*, 100620. https://doi.org/10.1016/J.JWPE.2018.04.017

Chougui, A., Zaiter, K., Belouatek, A., & Asli, B. (2014). Heavy metals and color retention by a synthesized inorganic membrane. *Arabian Journal of Chemistry*, *7*(5), 817–822. https://doi.org/10.1016/J.ARABJC.2012.11.017

Gan, G., Fan, S., Li, X., Zhang, Z., & Hao, Z. (2023). Adsorption and membrane separation for removal and recovery of volatile organic compounds. *Journal of Environmental Sciences*, *123*, 96–115. https://doi.org/10.1016/J.JES.2022.02.006

Gan, Y., Ding, C., Xu, B., Liu, Z., Zhang, S., Cui, Y., Wu, B., Huang, W., & Song, X. (2023). Antimony (Sb) pollution control by coagulation and membrane filtration in water/wastewater treatment: A comprehensive review. *Journal of Hazardous Materials*, *442*, 130072. https://doi.org/10.1016/J.JHAZMAT.2022.130072

Hafani, M., Chemrak, M. A., Djennad, M., & Benachour, D. (2021). Formulation and characterization of a new PET-based membrane for methane gas dehydration. *Polymer-Plastics Technology and Materials*, *60*(15), 1605–1619. https://doi.org/10.1080/25740881.2021.1912091

Johnson, C. J., & Singer, P. C. (2004). Impact of a magnetic ion exchange resin on ozone demand and bromate formation during drinking water treatment. *Water Research*, *38*(17), 3738–3750. https://doi.org/10.1016/J.WATRES.2004.06.021

Kammakakam, I., & Lai, Z. (2023). Next-generation ultrafiltration membranes: A review of material design, properties, recent progress, and challenges. *Chemosphere*, *316*, 137669. https://doi.org/10.1016/J.CHEMOSPHERE.2022.137669

Li, B., Qi, B., Guo, Z., Wang, D., & Jiao, T. (2023). Recent developments in the application of membrane separation technology and its challenges in oil-water separation: A review. *Chemosphere*, *327*, 138528. https://doi.org/10.1016/J.CHEMOSPHERE.2023.138528

Mahmoud, A. E. D., & Mostafa, E. (2023). Nanofiltration Membranes for the Removal of Heavy Metals from Aqueous Solutions: Preparations and Applications. *Membranes 2023, Vol. 13, Page 789*, *13*(9), 789. https://doi.org/10.3390/MEMBRANES13090789

Masturi, Widodo, R. D., Edie, S. S., Amri, U., Sidiq, A. L., Alighiri, D., Wulandari, N. A., Susilawati, & Amanah, S. N. (2018). Performance of zeolite ceramic membrane synthesized by wet mixing method as methylene blue dye wastewater filter. *Journal of Physics: Conference Series*, *983*(1), 012001. https://doi.org/10.1088/1742-6596/983/1/012001

Men, Y., Li, Z., Zhu, L., Wang, X., Cheng, S., & Lyu, Y. (2023). New insights into membrane fouling during direct membrane filtration of municipal wastewater and fouling control with mechanical strategies. *Science of The Total Environment*, *869*, 161775. https://doi.org/10.1016/J.SCITOTENV.2023.161775

Obada, D. O., Dodoo-Arhin, D., Dauda, M., Anafi, F. O., Ahmed, A. S., & Ajayi, O. A. (2017). The impact of kaolin dehydroxylation on the porosity and mechanical integrity of kaolin based ceramics using different pore formers. *Results in Physics*, *7*, 2718–2727. https://doi.org/10.1016/J.RINP.2017.07.048

Oliveira Neto, G. L., Oliveira, N. G. N., Delgado, J. M. P. Q., Nascimento, L. P. C., Magalhães, H. L. F., de Oliveira, P. L., Gomez, R. S., Farias Neto, S. R., & Lima, A. G. B. (2021). Hydrodynamic and Performance Evaluation of a Porous Ceramic Membrane Module Used on the Water–Oil Separation Process: An Investigation by CFD. *Membranes*, *11*(2), 1–25. https://doi.org/10.3390/MEMBRANES11020121

Pezeshki, H., Hashemi, M., & Rajabi, S. (2023). Removal of arsenic as a potentially toxic element from drinking water by filtration: A mini review of nanofiltration and reverse osmosis techniques. *Heliyon*, *9*(3), e14246. https://doi.org/10.1016/j.heliyon.2023.e14246

Puertas, G., Cazón, P., & Vázquez, M. (2023). Application of UV-VIS-NIR spectroscopy in membrane separation processes for fast quantitative compositional analysis: A case study of egg products. *LWT*, *174*, 114429. https://doi.org/10.1016/J.LWT.2023.114429

Rafya, M., Misrar, W., Saâdi, L., Mansori, M., Waqif, M., Hafidi, A., Zehhar, N., & Benkhalti, F. (2023). Ceramic membrane support based on kaolin and solid waste from hydrodistillation of

Rosmarinus officinalis L. *Materials Chemistry and Physics*, *295*, 127030. https://doi.org/10.1016/J.MATCHEMPHYS.2022.127030

Ramutshatsha-Makhwedzha, D., & Nomngongo, P. N. (2022). *Application of Ultrafiltration Membrane Technology for Removal of Dyes from Wastewater*. 37–47. https://doi.org/10.1007/978-981-16-4823-6_3

Rezende Moreira, V., Abner Rocha Lebron, Y., & Cristina Santos Amaral, M. (2022). Enhancing industries exploitation: Integrated and hybrid membrane separation processes applied to industrial effluents beyond the treatment for disposal. *Chemical Engineering Journal*, *430*, 133006. https://doi.org/10.1016/J.CEJ.2021.133006

Santra, B., Ramrakhiani, L., Kar, S., Ghosh, S., & Majumdar, S. (2020). Ceramic membrane-based ultrafiltration combined with adsorption by waste derived biochar for textile effluent treatment and management of spent biochar. *Journal of Environmental Health Science and Engineering*, *18*(2), 973. https://doi.org/10.1007/S40201-020-00520-W

Shoshaa, R., Ashfaq, M. Y., & Al-Ghouti, M. A. (2023). Recent developments in ultrafiltration membrane technology for the removal of potentially toxic elements, and enhanced antifouling performance: A review. *Environmental Technology & Innovation*, *31*, 103162. https://doi.org/10.1016/J.ETI.2023.103162

Sutariya, B., Sargaonkar, A., & Raval, H. (2023). Methods of visualizing hydrodynamics and fouling in membrane filtration systems: recent trends. *Separation Science and Technology*, *58*(1), 101–130. https://doi.org/10.1080/01496395.2022.2089585

Zaiter, K., Belouatek, A., Asli, B., & Szymczyk, A. (2020). Application and Treatment of Dye Congo Red, Metal and COD Retention by Modified Membranes Texture. *Journal of Advanced Research in Fluid Mechanics and Thermal Sciences*, *72*(2), 13–24. https://doi.org/10.37934/arfmts.72.2.1324

Zaiter, K., Belouatek, A., Chougui, A., Asli, B., & Szymczyk, A. (2015). Color, COD, and salt retention by inorganic membrane. *Desalination and Water Treatment*, *53*(1), 66–72. https://doi.org/10.1080/19443994.2013.838525

Zanurin, A., Johari, N. A., Alias, J., Ayu, H. M., Redzuan, N., & Izman, S. (2022). Research progress of sol-gel ceramic coating: A review. *Materials Today: Proceedings*, *48*, 1849–1854. https://doi.org/10.1016/J.MATPR.2021.09.203

Zhao, C., Xu, X., Chen, J., & Yang, F. (2013). Effect of graphene oxide concentration on the morphologies and antifouling properties of PVDF ultrafiltration membranes. *Journal of Environmental Chemical Engineering*, *1*(3), 349–354. https://doi.org/10.1016/J.JECE.2013.05.014